AEDC-TR-76-123

Cy 5

CALCULATION OF THE LAMINAR VISCOUS SHOCK LAYER ON A BLUNT BICONIC BODY AT INCIDENCE TO SUPERSONIC AND HYPERSONIC FLOW

VON KÁRMÁN GAS DYNAMICS FACILITY
ARNOLD ENGINEERING DEVELOPMENT CENTER
AIR FORCE SYSTEMS COMMAND
ARNOLD AIR FORCE STATION, TENNESSEE 37389

December, 1976

Final Report for Period July 1, 1975 — June 1976

Approved for public release; distribution unlimited.

Prepared for

DIRECTORATE OF TEST (XO)
ARNOLD ENGINEERING DEVELOPMENT CENTER
ARNOLD AIR FORCE STATION, TENNESSEE 37389

NOTICES

When U. S. Government drawings specifications, or other data are used for any purpose other than a definitely related Government procurement operation, the Government thereby incurs no responsibility nor any obligation whatsoever, and the fact that the Government may have formulated, furnished, or in any way supplied the said drawings, specifications, or other data, is not to be regarded by implication or otherwise, or in any manner licensing the holder or any other person or corporation, or conveying any rights or permission to manufacture, use, or sell any patented invention that may in any way be related thereto.

Qualified users may obtain copies of this report from the Defense Documentation Center.

References to named commercial products in this report are not to be considered in any sense as an endorsement of the product by the United States Air Force or the Government.

This report has been reviewed by the Information Office (OI) and is releasable to the National Technical Information Service (NTIS). At NTIS, it will be available to the general public, including foreign nations.

APPROVAL STATEMENT

This technical report has been reviewed and is approved for publication.

FOR THE COMMANDER

Keith L. Kushman

KEITH L. KUSHMAN
Captain, USAF
Analysis and Evaluation Division
Directorate of Test

Alan L Devereaux

ALAN L. DEVEREAUX
Colonel, USAF
Director of Test

REPORT DOCUMENTATION PAGE		READ INSTRUCTIONS BEFORE COMPLETING FORM
1 REPORT NUMBER AEDC-TR-76-123	2 GOVT ACCESSION NO.	3 RECIPIENT'S CATALOG NUMBER
4 TITLE (and Subtitle) CALCULATION OF THE LAMINAR VISCOUS SHOCK LAYER ON A BLUNT BICONIC BODY AT INCIDENCE TO SUPERSONIC AND HYPERSONIC FLOW		5 TYPE OF REPORT & PERIOD COVERED Final Report-July 1, 1975 - June 1976 6 PERFORMING ORG REPORT NUMBER
7 AUTHOR(s) Arloe W. Mayne, Jr., ARO, Inc.		8 CONTRACT OR GRANT NUMBER(s)
9 PERFORMING ORGANIZATION NAME AND ADDRESS Arnold Engineering Development Center (XO) Air Force Systems Command Arnold Air Force Station, Tennessee 37389		10 PROGRAM ELEMENT, PROJECT, TASK AREA & WORK UNIT NUMBERS Program Element 63311F System 627A
11 CONTROLLING OFFICE NAME AND ADDRESS Arnold Engineering Development Center (DYFS) Arnold Air Force Station, Tennessee 37389		12 REPORT DATE December 1976 13 NUMBER OF PAGES 31
14 MONITORING AGENCY NAME & ADDRESS(if different from Controlling Office)		15 SECURITY CLASS (of this report) UNCLASSIFIED 15a DECLASSIFICATION/DOWNGRADING SCHEDULE N/A

16 DISTRIBUTION STATEMENT (of this Report)

Approved for public release; distribution unlimited.

17 DISTRIBUTION STATEMENT (of the abstract entered in Block 20, if different from Report)

18 SUPPLEMENTARY NOTES

Available in DDC

19 KEY WORDS (Continue on reverse side if necessary and identify by block number)

computations
layers (laminar, viscous)
shock (mechanics)
blunt bodies (biconic)
occurrence
supersonic flow
hypersonic flow

20 ABSTRACT (Continue on reverse side if necessary and identify by block number)

A fully viscous shock layer computation method developed by others to treat laminar flow over a sharp cone at incidence to a supersonic or hypersonic free stream has been extended to consider the case of flow over a blunt biconic configuration at angle of attack. The basic method treats the flow between the body surface and the bow shock wave by one set of equations which are valid in both the viscous and inviscid flow regions. A description is

DD FORM 1 JAN 73 1473 EDITION OF 1 NOV 65 IS OBSOLETE

20. ABSTRACT (Continued)

given of the computational methods used, particularly the method developed to treat the viscous shock layer over the spherical nose and the method used to take data from the end of the fore-cone solution to provide initial data for starting the aft-cone solution. Results from calculations which have been performed using the method developed in this investigation are compared with results from boundary-layer and inviscid flow calculations and with experimental data. The present technique is validated by the good agreement between the computed data and experimental data.

AFSC
Arnold AFS Tenn

PREFACE

The work reported herein was conducted by the Arnold Engineering Development Center (AEDC), Air Force Systems Command (AFSC), under Program Element 63311F, System 627A. The results were obtained by ARO, Inc. (a subsidiary of Sverdrup & Parcel and Associates, Inc.), contract operator of AEDC, AFSC, Arnold Air Force Station, Tennessee, under ARO Project Numbers V43A-07A, V41C-D3A, and V41C-B0A. The author of this report was Arloe W. Mayne, Jr., ARO, Inc. The data analysis was completed in June 1976. The manuscript (ARO Control No. ARO-VKF-TR-76-66) was submitted for publication on June 28, 1976.

Acknowledgment and thanks are extended to Mr. R. H. Eaves, ARO, Inc., for the experimental data used in Section 3.2, and to Messrs. L. D. Carter, D. E. Boylan, and W. T. Strike, all of ARO, Inc., who obtained the experimental data used in Sections 3.4 and 3.5. Appreciation is also due Mr. E. O. Marchand and Dr. J. C. Adams, Jr., ARO, Inc., who provided theoretical inviscid flow solutions.

CONTENTS

ILLUSTRATIONS

Figure

Figure | Page

1.0 INTRODUCTION

The accurate calculation of the aerodynamic behavior, surface heating, pressure and friction forces, etc., of wind tunnel models and flight vehicles requires the use of sophisticated methods which are almost inevitably embodied in digital computer codes. The calculation of the flow over an aerodynamic body is usually divided into the calculation of an inviscid flow field and the calculation of a viscous flow field, or boundary layer, over the body.

For the cases of supersonic and hypersonic flow which are of interest in this work, effective methods have been developed for solving the governing equations for both inviscid and viscous flow for two-dimensional and axisymmetric flows (e.g., Refs. 1 and 2). This is especially true for laminar flows, although numerous schemes have also been developed for turbulent boundary layers. For those situations in which the boundary layer is sufficiently thick to influence the external inviscid flow, iterative methods have been developed which couple the inviscid and viscous flow calculations through an effective-body concept, as in Ref. 3. A more rigorous treatment of this interaction problem, and of the entropy-layer swallowing problem discussed in Ref. 4, is inherent in the viscous shock layer methods, typified by Ref. 5, which treat the entire region between the body and bow shock by solving one set of equations which are valid in both the viscous and inviscid regions.

For the case of more complex flow, in particular the case of flow over an axisymmetric body at incidence to a supersonic or hypersonic stream, the calculation methods essentially parallel those for the two-dimensional and axisymmetric flow situations, although the complexity of the methods is increased considerably for this three-dimensional flow problem. Calculation methods for inviscid and viscous flows over axisymmetric bodies at incidence are described in Refs. 6 and 7, for example, and Ref. 8 describes a viscous shock layer method which has been developed to treat the complete viscous and inviscid flow over a right circular cone at incidence to a supersonic or hypersonic free stream. This last method has been used by Adams and Griffith (Ref. 9) to study the static stability characteristics of a sharp cone at angle of attack under hypersonic flow conditions. They show that, even under laminar flow conditions, the viscous shock layer treatment (as opposed to a coupled inviscid/boundary-layer scheme) is necessary to provide accurate, or even qualitatively correct, results for this problem.

Generally speaking, the methods for three-dimensional flows discussed in the previous paragraph are not nearly as well developed or as widely applied as the corresponding methods for two-dimensional and axisymmetric flows. This report presents a technique which has been developed for the application of the viscous shock layer method of Ref. 8 to the calculation of the laminar shock layer on a blunt biconic body at incidence to supersonic and hypersonic flow. A companion experimental program has also been undertaken, and data from those experiments and other sources are compared with results from the present investigation to validate the approach taken.

2.0 THEORETICAL METHODS

The viscous shock layer method developed by Lubard and Helliwell (Ref. 8), hereinafter referred to as the Hypersonic Viscous Shock Layer (HVSL) code, is applicable only to flow over frustums of right circular cones. In order to compute the flow over a blunt biconic body, it was necessary to develop a method to treat the nose cap shock layer, transform the results into a form to begin the fore-cone shock layer solution, and then to take data from the end of the fore-cone shock layer solution and transform it into a form to begin the aft-cone shock layer solution. This procedure is indicated schematically in Fig. 1. The following sections give a brief description of the HVSL code and the methods developed to use in calculating the laminar shock layer over a spherically blunted biconic body.

2.1 HYPERSONIC VISCOUS SHOCK LAYER

Probably the best method currently available for treating supersonic and hypersonic flow over cone frustums at angle of attack is the three-dimensional viscous shock layer approach of Ref. 8. An approximate system of governing equations is obtained by assuming that the viscous, streamwise derivative terms are small compared with the viscous normal and circumferential derivatives. The resulting equations are valid in both the inviscid and viscous regions including any circumferential separation zone which may develop on the leeward side at higher angles of attack (greater than approximately the cone semivertex angle). Since this set of governing partial differential equations is parabolic in the streamwise direction, a marching-type numerical solution technique is used. An implicit finite-difference treatment is

applied to the normal derivatives in conjunction with Newton's method of iteration for solution of the nonlinear algebraic equations which result from differencing of the circumferential derivatives. The equations are solved between the body surface and the bow shock; boundary conditions at the shock and its resulting shape are calculated by using the Rankine-Hugoniot shock-crossing relations and a one-sided differencing of the continuity equation. A thermally and calorically perfect air model is used having a constant specific heat ratio $\gamma = 1.40$ in conjunction with the Sutherland viscosity law and a constant laminar Prandtl number of 0.71. The actual digital computer code is documented in the report by Helliwell and Lubard (Ref. 10).

It is important to note and appreciate that the hypersonic viscous shock layer approach treats both the inviscid and viscous regions of the flow field with one composite set of equations. Hence, complicated inviscid-viscous interactions which occur under hypersonic flow conditions are automatically included in the analysis; the need for explicit treatment of higher-order boundary-layer effects such as displacement-induced pressure which require tedious matching of separate inviscid and boundary-layer solutions is eliminated.

2.2 SPHERICAL NOSE CAP SHOCK LAYER

The method devised to compute the shock layer flow over the spherical nose cap is based on the assumption that the flow there is axisymmetric in a wind-axis coordinate system. In a calculation of the inviscid flow over the body, this is equivalent to requiring that the flow over the nose cap become supersonic before the sphere-cone tangency is reached, and this condition was also required for all of the calculations made in this study.

The shock layer method used to obtain the flow field over the hemispherical nose cap was based on the method of Ref. 11 for computing boundary-layer flows, including normal pressure gradient and longitudinal curvature effects. A basically pragmatic approach was followed in which the continuity equation, x-momentum equation, and total enthalpy form of the energy equation as given below were solved using a normalized von Mises coordinate system and a marching implicit finite difference solution method (see Ref. 11 for details of solution method).

Continuity Equation:

$$\partial/\partial x(\rho u r) + \partial/\partial y\,[(1 + \kappa y)\,\rho v r] = 0 \tag{1}$$

x-Momentum Equation:

$$\rho u(\partial u/\partial x) + \rho v(1 + \kappa y)\,\partial u/\partial y + \rho u v \kappa = - \partial p/\partial x + 1/r\,\partial/\partial y\,[\mu r(1 + \kappa y)\,\partial u/\partial y] - \kappa u\,\partial\mu/\partial y \tag{2}$$

Energy Equation:

$$\rho u\,(\partial H/\partial x) + \rho v(1 + \kappa y)\,\partial H/\partial y = \frac{-\kappa\partial(\mu u^2)}{\partial y} + \frac{1}{r}\frac{\partial}{\partial y}\left[\frac{\mu r}{Pr}(1 + \kappa y)\frac{\partial H}{\partial y} + \frac{Pr - 1}{Pr}\mu r(1 + \kappa y)\frac{\partial(u^2/2)}{\partial y}\right] \tag{3}$$

These equations were solved to obtain v, u, and H. Because of difficulties encountered by other investigators and in preliminary work in this study in including the normal momentum equation and solving the entire hemisphere shock layer for other than very low Reynolds number flows, the pressure field was taken from a solution of the inviscid flow equations obtained using the method of Aungier (Ref. 12). The inviscid solution was also used to obtain the variation with x of the stream function value at the outer edge of the shock layer, and the shock wave shape for the purpose of obtaining through the Rankine-Hugoniot relations the outer (shock) boundary conditions on u. The surface boundary conditions required were H specified at the surface and u = v = 0 at the surface. The value of H at the shock was the free-stream value. The value of the shock layer thickness determined by the solution of Eqs. (1), (2), and (3) in von Mises coordinates was not generally the same as that obtained in the inviscid solution from the method of Ref. 12, and for that reason the pressure field data were used in terms of y/y_{sh}, where this coordinate varied from 0 at the surface to 1.0 at the shock in both cases.

Figure 2 indicates the method used to obtain the initial starting data for the HVSL code at the sphere-cone tangency location. An axisymmetric flow solution, obtained by the methods just discussed, was found for the meridian 0-1. Starting data for the HVSL code is composed of flow-field data on surface normals at a series of locations around the sphere-cone tangency 1-2. A typical location is "b" where, because of the axisymmetric nature of the flow on the nose, the flow is identical to that at "a." In order to use the solution from "a" at "b", it is necessary to properly nondimensionalize the variables and trans-

form the velocity data from a wind-axis coordinate form to a body-axis coordinate form.

In Ref. 13, sphere-cone tangency starting data for the HVSL code were determined by obtaining separate inviscid and boundary-layer solutions over the nose cap and merely adding the inviscid profiles to the boundary-layer profiles. Entropy layer swallowing by the boundary layer was neglected, and questionable behavior of the normal slopes of the flow field variables at the boundary-layer edge also occurred. The present method of treating this problem is felt to be superior to that of Ref. 13, although much room for improvement still remains, especially for any other than high Reynolds number cases.

2.3 AFT–CONE STARTING DATA

The HVSL code is used to obtain the flow field along body normals over the fore cone at a series of x locations along the body, treating a series of ϕ locations (measured around the body from the windward side) at each station along the body. The fore-cone solution is extended beyond the end of the actual fore cone to give sufficient data that aft-cone surface normal interpolations can be carried from the body to the bow shock. This procedure, shown in Fig. 3, is carried out at each ϕ location to yield a set of starting data for the HVSL solution over the aft cone. Also, at this point the velocity components must be transformed from fore-cone surface coordinates to aft-cone surface coordinates.

3.0 RESULTS OF CALCULATIONS

In this section, results from calculations made using the present method are compared with results from boundary-layer and inviscid flow calculations and with experimental data. The method used to treat the nose region is examined by comparing flow-field data with results from an inviscid flow calculation method, and by comparing surface heating data with boundary-layer results and experimental data. The shock layer method used for the biconic afterbody is validated by comparing results from the present method with experimental data, and viscous influences on surface pressure data are examined by making comparisons with results of inviscid flow calculations.

All of the calculations (inviscid and viscous) made in this investigation treated the gas as thermally and calorically perfect air and were performed on an IBM 370/165 digital computer.

3.1 HEMISPHERE SHOCK LAYER FLOW FIELD

Figures 4 and 5 compare flow-field results for a 1-in.-radius hemisphere in a Mach 10 flow obtained using the method described in Section 2.2 with inviscid flow results obtained using the method of Ref. 12. The wall temperature was 540°R, the free-stream Reynolds number (based on nose radius) was 3.75×10^5, and the free-stream total temperature was 2,050°R.

Figure 4 compares flow-field profiles from the nose region viscous shock layer calculations with inviscid flow calculation results. These results are for the 90-deg location on the hemisphere, with respect to the stagnation location. As can be seen in the u velocity profile, the region of viscous influence (boundary layer) occupies less than ten percent of the shock layer thickness for this case. Outside the region of viscous influence, there is reasonably good agreement between the two sets of results for the density, normal velocity, and tangential velocity, although the computed thickness of the viscous shock layer is approximately five percent less than the thickness of the inviscid flow field.

Figure 5 shows the inviscid flow shock and the computed edge of the viscous shock layer over the surface of the hemisphere, from the stagnation point to the 90-deg location. Except for an excursion in the viscous shock layer thickness near the stagnation point, the two thicknesses agree well over the entire hemisphere. The reason for the excursion is not understood; however, since the region of the viscous shock layer used in providing initial data for the HVSL code does not begin until about 50 deg around the hemisphere ($z/r_n = 0.357$), the excursion's effect on the initial data is felt to be small.

3.2 HEMISPHERE CYLINDER SURFACE HEATING

Figure 6 shows the surface heating rate distribution (in Stanton number form) over a 2.90-in.-radius hemisphere cylinder at zero angle of attack in a Mach 8 flow. Viscous shock layer results obtained using the present method, boundary-layer results obtained using the method

of Ref. 2, and experimental data taken in the AEDC von Kármán Gas Dynamics Facility (VKF) Hypersonic Wind Tunnel (B) are presented. The free-stream Reynolds number, based on the nose radius, was 8.55×10^5, the free-stream total temperature was 1,335°R, and the wall temperature was approximately 540°R. The agreement among the data from the three sources is quite reasonable on both the hemisphere and the cylinder portions of the body.

The comparisons shown in Figs. 4 through 6 show that the present treatment of the nose region shock layer is generally valid, and the cylinder section results in Fig. 6 indicate that the HVSL results obtained using the nose region final data as starting data are reasonable. The following two sections present more detailed results from HVSL code for a sphere cone and blunt biconics at incidence to hypersonic free streams.

3.3 HEATING DATA ON BLUNT BICONIC AT INCIDENCE

Figure 7 shows a comparison of the heat-transfer distribution measured (Ref. 14) on a 15.1-deg/11.3-deg blunt biconic at 5-deg incidence to a Mach 10.23 free stream with that computed by the present methods. The model nose radius was 0.24 in., the free-stream Reynolds number (based on nose radius) was 29,400, the free-stream total temperature was 1,825°R, and a wall temperature of 540°R was used. The data are presented as the ratio of the local heat-transfer coefficient to a reference heat-transfer coefficient, where the reference value h_o is 0.0313 Btu/(ft^2-sec-°R). The adiabatic wall temperature needed to form the heat-transfer coefficient was computed using a recovery factor of 0.84 and edge conditions determined by assuming the air to have expanded from normal shock conditions to a pressure defined by the tangent-cone approximations.

Figure 7a shows circumferential heat-transfer distributions at two locations on the fore cone and two locations on the second conical frustum. Figure 7b shows longitudinal distributions along the windward and leeward sides and along the ϕ = 90-deg line midway between the windward and leeward sides. Except for some discrepancy on the windward side near the front of the body, the measured and computed heating agree quite well in both the circumferential and longitudinal comparisons.

3.4 PRESSURE DATA ON SPHERE CONE AT INCIDENCE

Figures 8 through 10 show surface pressure and pitot pressure profile data on a 4-deg sphere cone at 3-deg incidence to a Mach 9.8 free stream. The experimental data shown in these figures were obtained in the AEDC/VKF Hypersonic Wind Tunnel (C) as part of the investigation reported in Ref. 15. The model nose radius was 0.281 in., and the base radius was 1.25 in. The free-stream Reynolds number (based on nose radius) was 9,200, the free-stream total temperature was 1,893°R, and the model surface temperature was 1,075°R.

Figure 8 compares the present HVSL surface pressure results with experimental data and with results from the inviscid calculation method of Ref. 16. This figure shows a significant viscous influence on the surface pressure level, especially on the lee side where the experimental data and HVSL results are some 30 percent above the computed inviscid level.

Figure 9 compares circumferential distributions of the surface pressure computed by the present method with the measured values. The discrepancy between the two sets of data at the tap 1 location, which is near the sphere-cone tangency, may be caused by inadequacies in the nose starting solution at this relatively low Reynolds number condition since the method used in this study does not consider viscous effects on the nose cap pressure distribution. At the three locations farther down the body, there is good agreement between the measured and computed pressure levels around the body, indicating that the HVSL method has properly treated the viscous influences on the pressure level.

Figure 10 compares impact pressure profile data computed using the HVSL method with experimental data. The data are for a location in the lee-side symmetry plane near the base of the model, and there is quite good agreement between the calculations and the measurements. The shock location and the edge of the viscous layer shown in Fig. 10 were determined from HVSL calculations. The shock location is a direct result of the calculations, and the edge of the viscous layer was determined by examining the total enthalpy profile. The edge of the viscous layer was defined to be the point where the total enthalpy essentially reached the free-stream value, examining the profile from the wall outward.

3.5 PRESSURE DATA ON BLUNT BICONIC AT INCIDENCE

Figures 11 through 13 show surface pressure and pitot pressure profile data on a 9.33/5.00-deg spherically blunted biconic at 2-deg incidence in a Mach 10.1 free stream. The experimental data shown in these figures were obtained in the AEDC/VKF Tunnel C. Descriptions of the wind tunnel, the instrumentation, and the test procedures are as given in Ref. 15. The model (sketched in Fig. 11) had a nose radius of 0.23 in. and a base radius of 1.50 in. The radius of the model at the junction of the two conical frustums was 0.755 in. The free-stream Reynolds number (based on the nose radius) was 35,000, the free-stream total temperature was 1,900°R, and the model surface temperature was approximately 1,340°R.

Figure 11 compares wind- and lee-side surface pressure data computed by the HVSL method with inviscid calculation results and with experimental data. Significant viscous effects are indicated by comparing the inviscid data with the HVSL results or the experimental data, especially on the lee side of the model. While the inviscid results are consistently below the experimental data, the present HVSL results agree quite well with the experimental data except for the point immediately past the cone-cone junction on the wind side. The HVSL results are also somewhat under the measurements at the first measuring station on the fore cone. In addition to shortcomings previously attributed to the method used for the spherical nose cap solution, the HVSL results are for a constant wall temperature model, and the fact that the actual model was hotter on the nose could have caused the measured pressures to be higher than computed in the nose region.

Figure 12 compares circumferential distributions of the surface pressure data as computed by the HVSL method with the experimental data. Data are compared at a location prior to the cone-cone junction (tap 3), at a location immediately downstream of the junction (tap 4), and at a location far down on the aft cone (tap 8). Excellent agreement is exhibited between the theoretical and measured data at the tap 3 and tap 8 locations. At the tap 4 location, just past the cone-cone junction, the computed pressure level is considerably less than the measured value. Thus, the calculations exhibit a somewhat more rapid expansion than do the experimental data, although the upstream levels and that downstream past the immediate neighborhood of the junction agree quite well. It is possible that this discrepancy could be lessened by application of more recent experience in manipulating the HVSL solution parameters, step sizes, etc., for the computations in this neighborhood.

Figure 13 compares pitot pressure profile data computed by the HVSL method with measurements made in the lee-side symmetry plane at the same three locations as the surface pressure data shown in Fig. 12. There is reasonably good agreement between the calculated and measured data at each location. The indicated shock locations are from the HVSL results.

4.0 SUMMARY AND CONCLUSIONS

The combination of the cone frustum laminar hypersonic viscous shock layer calculation method of Ref. 8 and the methods developed in this investigation to generate blunt nose starting data and to treat the biconic junction have been shown to yield a method which is applicable to the problem of computing the laminar viscous shock layer over a blunt biconic at incidence in a supersonic or hypersonic stream. The approach taken has been validated by the good agreement shown between the results of calculations made by the present method and measured surface heating data, surface pressure data, and impact pressure profile data.

Two improvements which should be made to the present method are obvious. First, a better treatment of the nose cap flow for low Reynolds number situations should be sought. Second, the HVSL method should be modified to allow the consideration of a variable wall temperature distribution.

In addition to these two improvements, it is currently planned to extend the HVSL method to allow the consideration of flows with turbulent boundary layers.

REFERENCES

1. Inouye, M., Rakich, J. V., and Lomax, H. "A Description of Numerical Methods and Computer Programs for Two-Dimensional and Axisymmetric Supersonic Flow over Blunt-Nosed and Flared Bodies." NASA TN D-2970, August 1965.

2. Mayne, A. W., Jr. and Dyer, D. F. "Comparisons of Theory and Experiment for Turbulent Boundary Layers on Simple Shapes at Hypersonic Conditions." Proceedings of the 1970 Heat Transfer and Fluid Mechanics Institute, Stanford University Press, 1970, pp. 168-188.

3. Mayne, A. W., Jr., Gilley, G. E., and Lewis, C. H. "Binary Boundary Layers on Sharp Cones in Low Density Supersonic and Hypersonic Flow." AEDC-TR-68-275 (AD682294), February 1969.

4. Mayne, A. W., Jr. and Adams, J. C., Jr. "Streamline Swallowing by Laminar Boundary Layers in Hypersonic Flow." AEDC-TR-71-32 (AD719748), March 1971.

5. Davis, R. T. "The Hypersonic Fully Viscous Shock-Layer Problem." Report SC-RR-68-840, Sandia Corporation, Albuquerque, New Mexico, 1968. See also AIAA Journal, Vol. 8, No. 5, May 1970, pp. 843-851.

6. Rakich, J. V. "A Method of Characteristics for Steady Three-Dimensional Supersonic Flow with Application to Inclined Bodies of Revolution." NASA TN D-5341, October 1969.

7. Mayne, A. W., Jr. "Calculation of the Boundary-Layer Flow in the Windward Symmetry Plane of a Spherically Blunted Axisymmetric Body at Angle of Attack, Including Streamline Swallowing Effects." AEDC-TR-73-166 (AD768340), October 1973.

8. Lubard, S. C. and Helliwell, W. S. "Calculation of the Flow on a Cone at High Angle of Attack." RDA-TR-150, R & D Associates, Santa Monica, California, February 1973. See also AIAA Journal, Vol. 12, No. 7, July 1974, pp. 965-974.

9. Adams, J. C., Jr. and Griffith, B. J. "Hypersonic Viscous Static Stability of a Sharp 5-Deg Cone at Incidence." AIAA Journal, Vol. 14, No. 8, August 1976.

10. Helliwell, W. S. and Lubard, S. C. "An Implicit Method for Three-Dimensional Viscous Flow with Application to Cones at Angle of Attack." TR-0074(4450-64)-1, The Aerospace Corporation, El Segundo, California, September 1973.

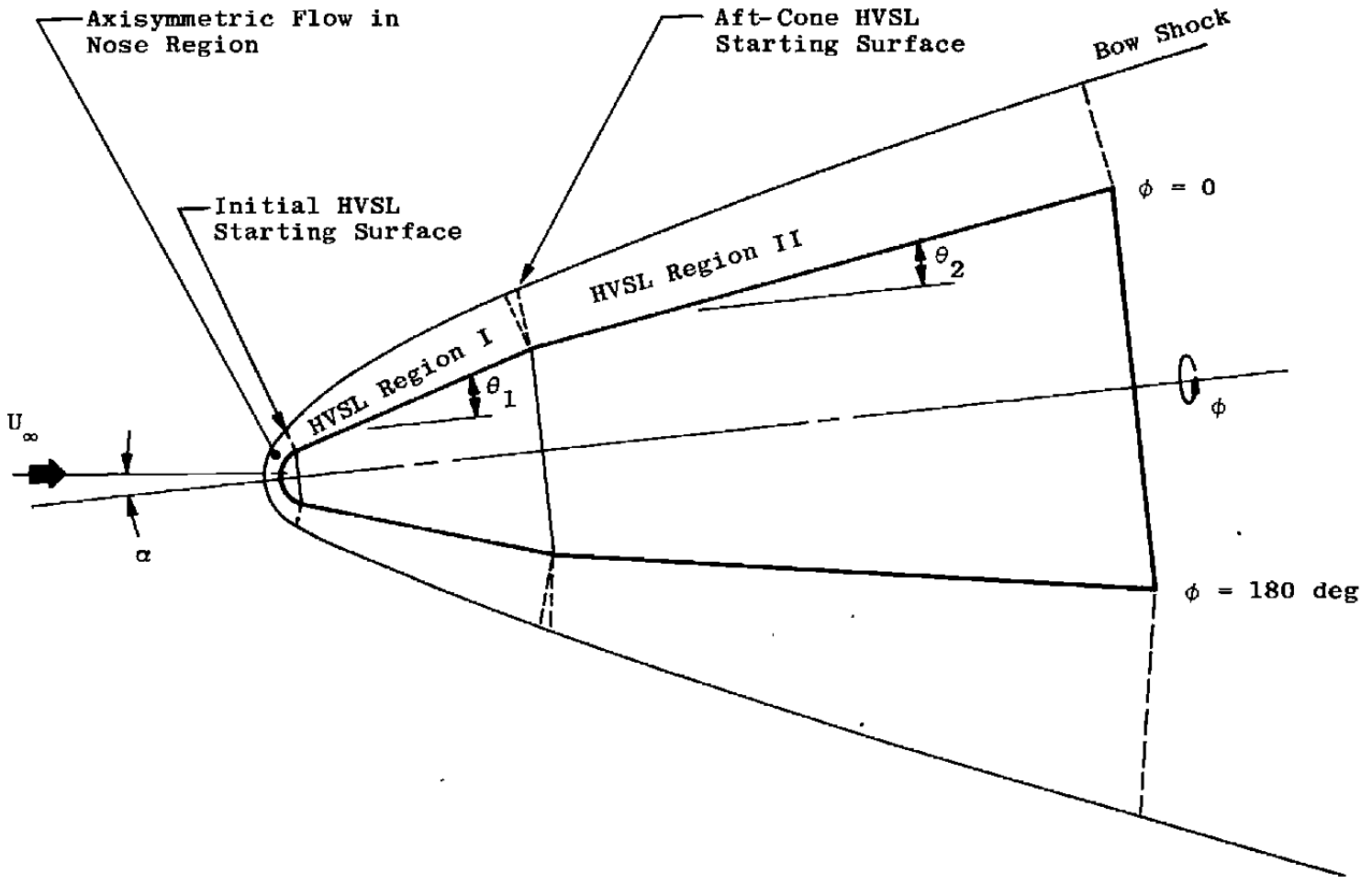

Figure 1. Overall schematic of blunt biconic shock layer treatment.

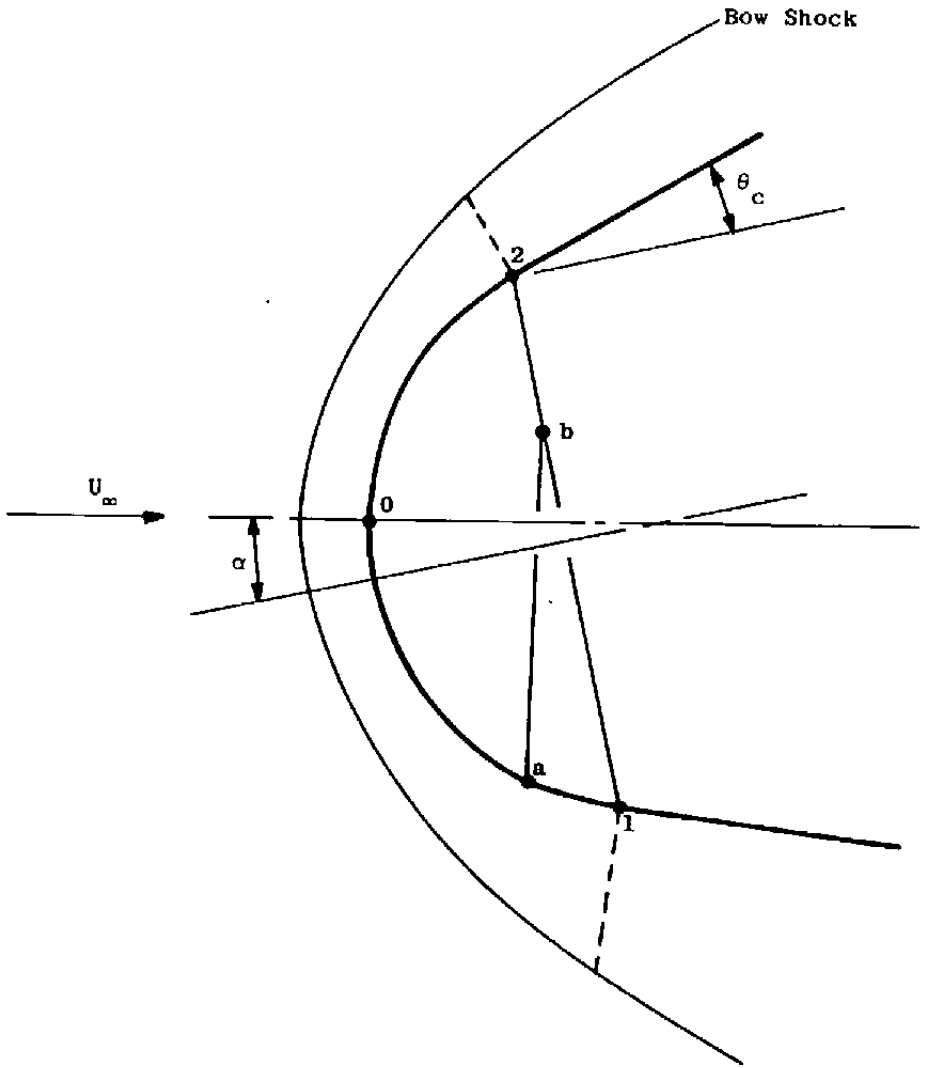

Nose Cap Flow Axisymmetric About Wind Axis

Axisymmetric Flow Solution from 0-1 Can Be Used to Provide Initial Data on 1-2, e.g., the Flow at "b" Is the Same As at "a"

(Solution on 1-2 Must Be Transformed to Body-Axis Coordinates)

Figure 2. Treatment of nose cap flow to yield initial HVSL starting data.

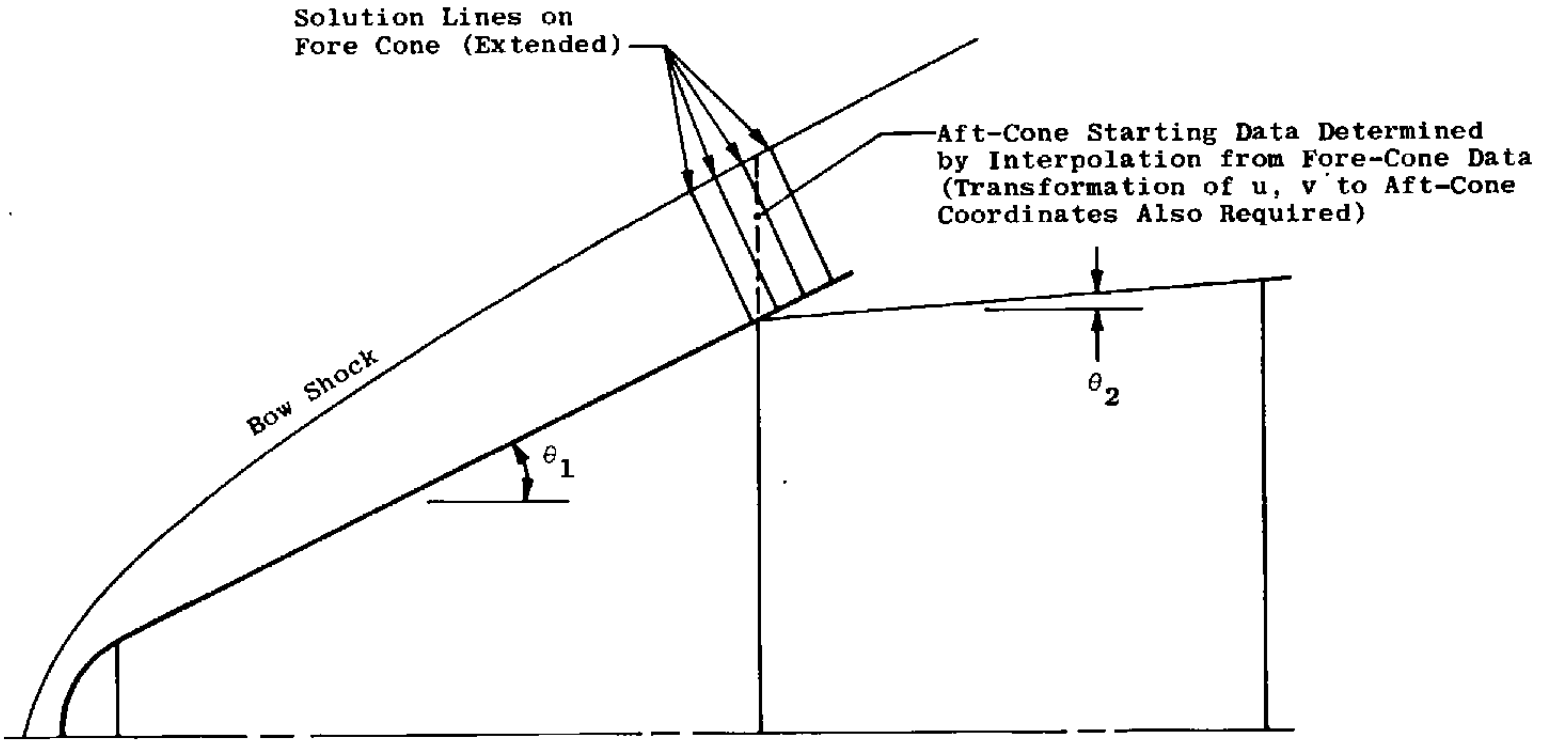

Figure 3. Determination of aft-cone starting data at a given ϕ location.

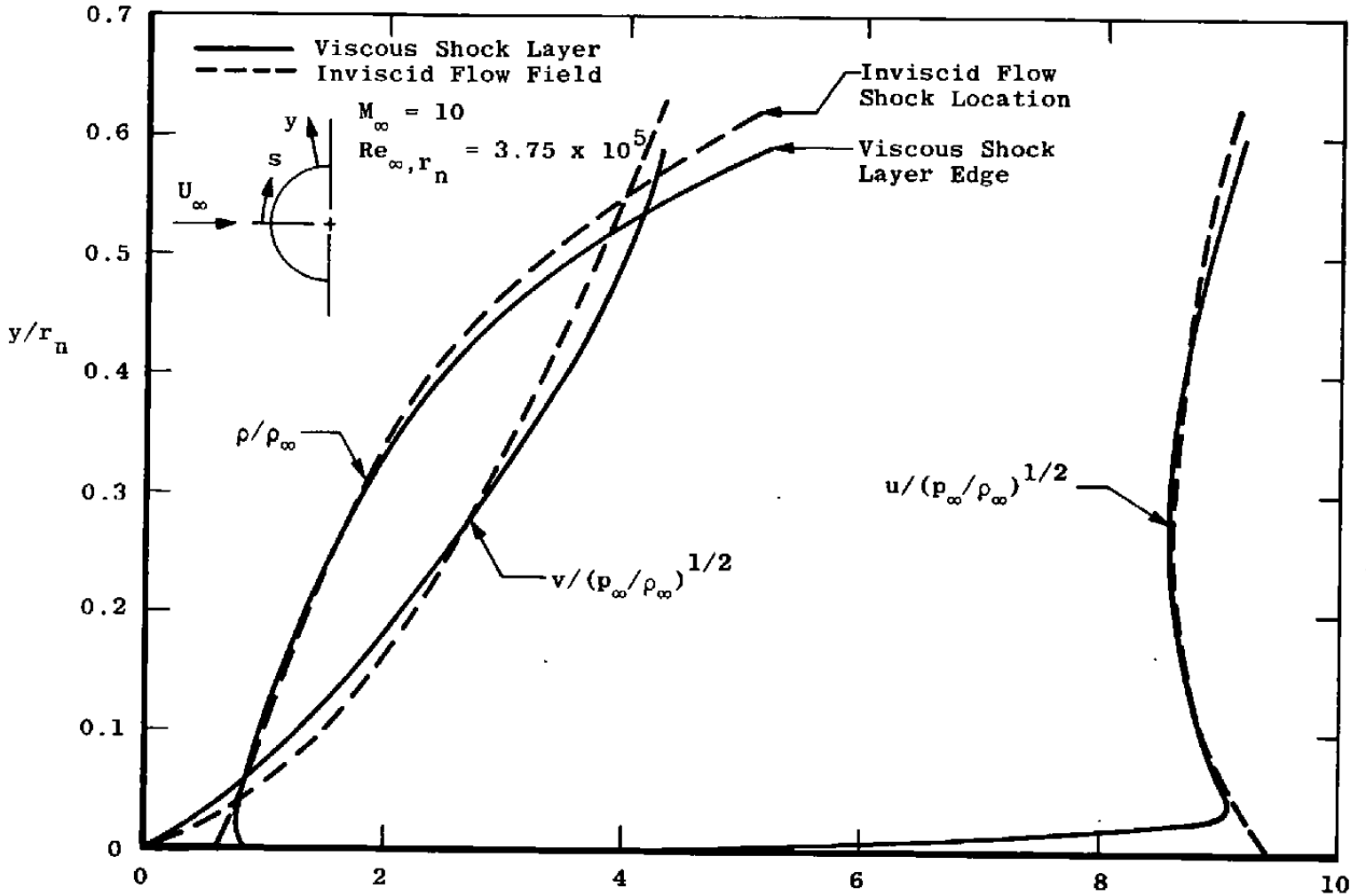

Figure 4. Flow-field data at s/r_n = 1.57 on hemisphere in a Mach 10 flow.

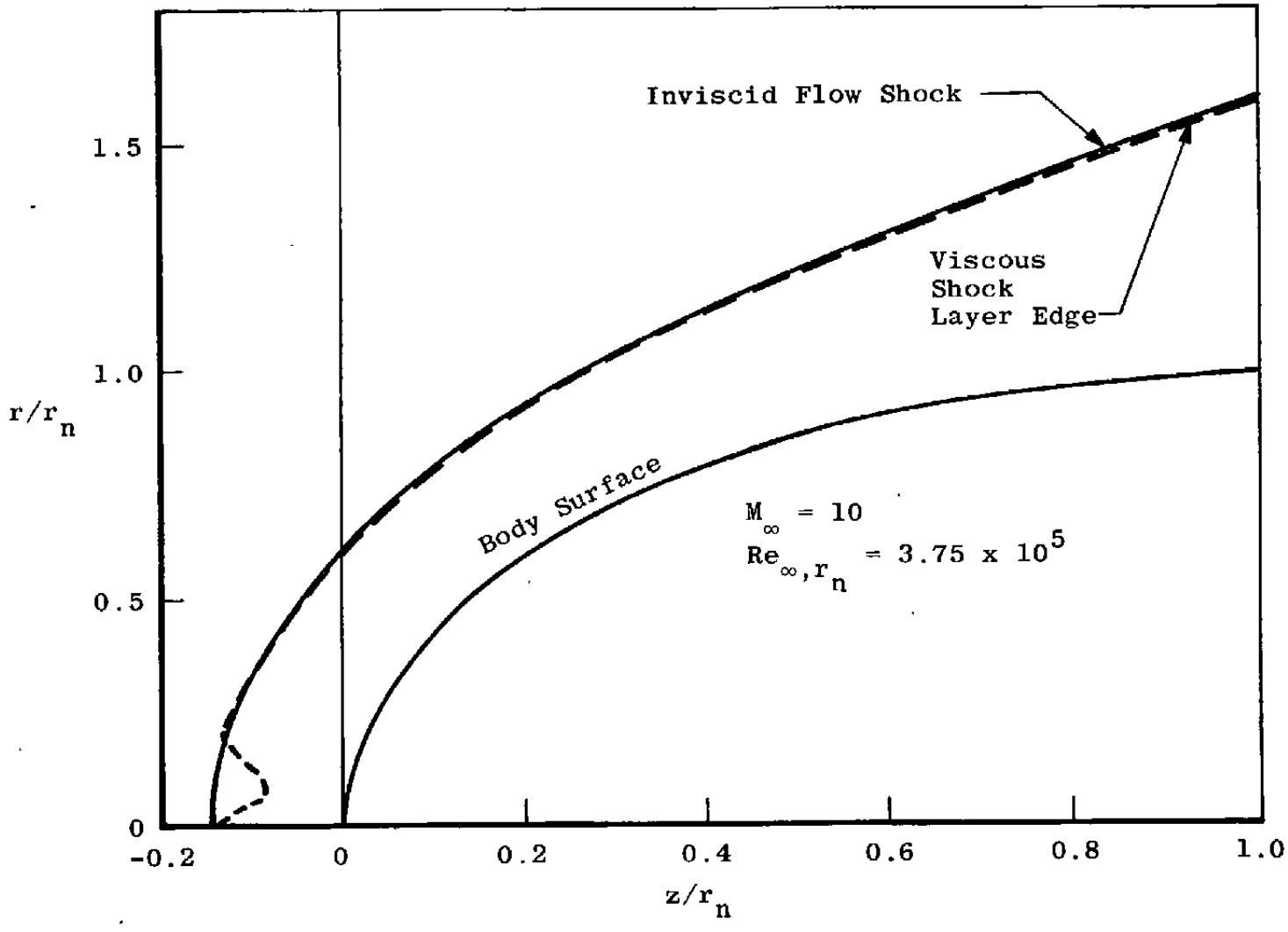

Figure 5. Inviscid flow shock and viscous shock layer edge comparison on hemisphere in a Mach 10 flow.

AEDC-TR-76-123

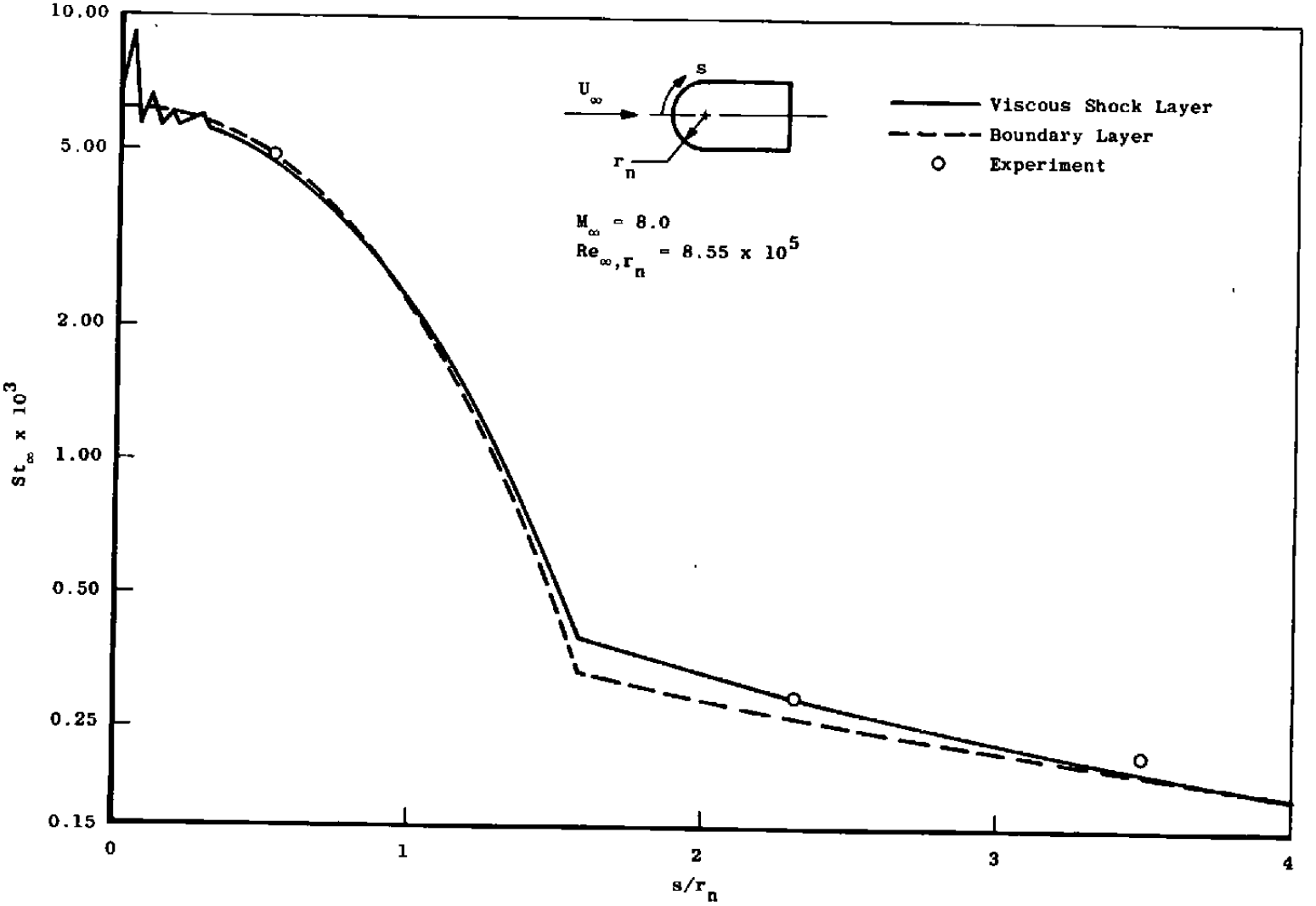

Figure 6. Stanton number distribution on a hemisphere cylinder in a Mach 8 flow.

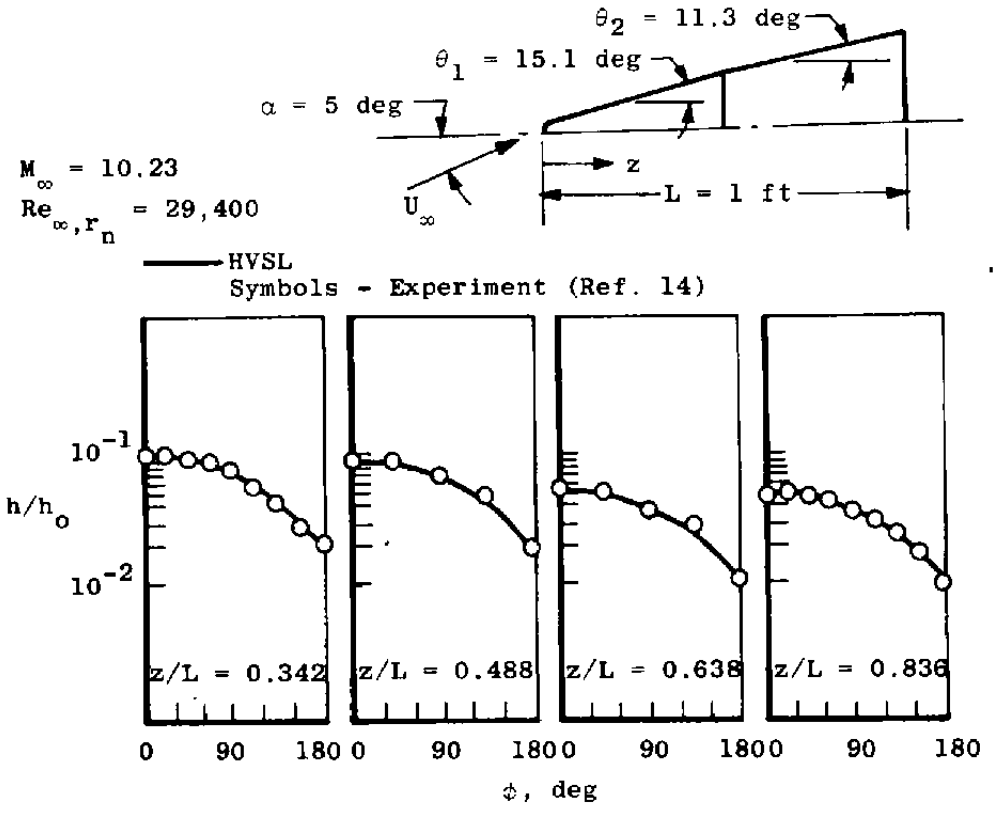

a. Circumferential distributions

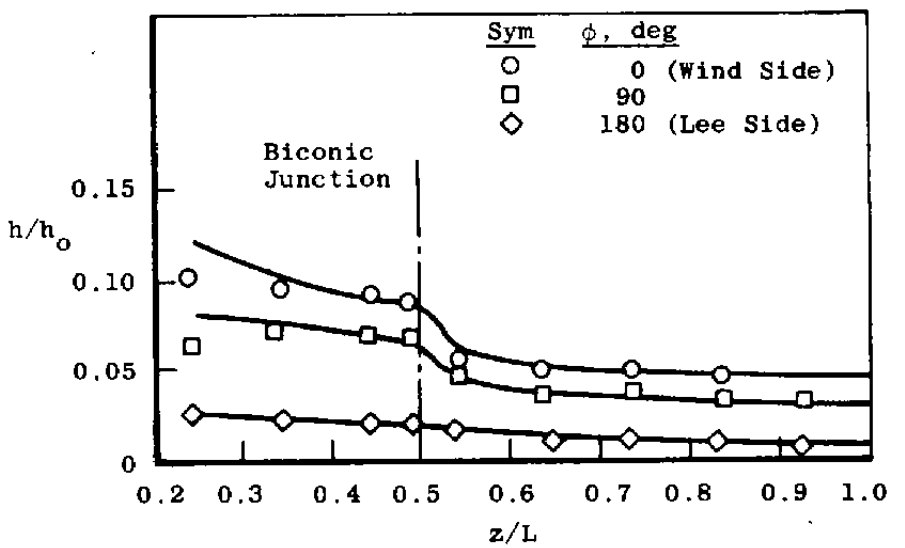

b. Longitudinal distributions

Figure 7. Heat-transfer distributions on a blunt biconic in a Mach 10.23 flow.

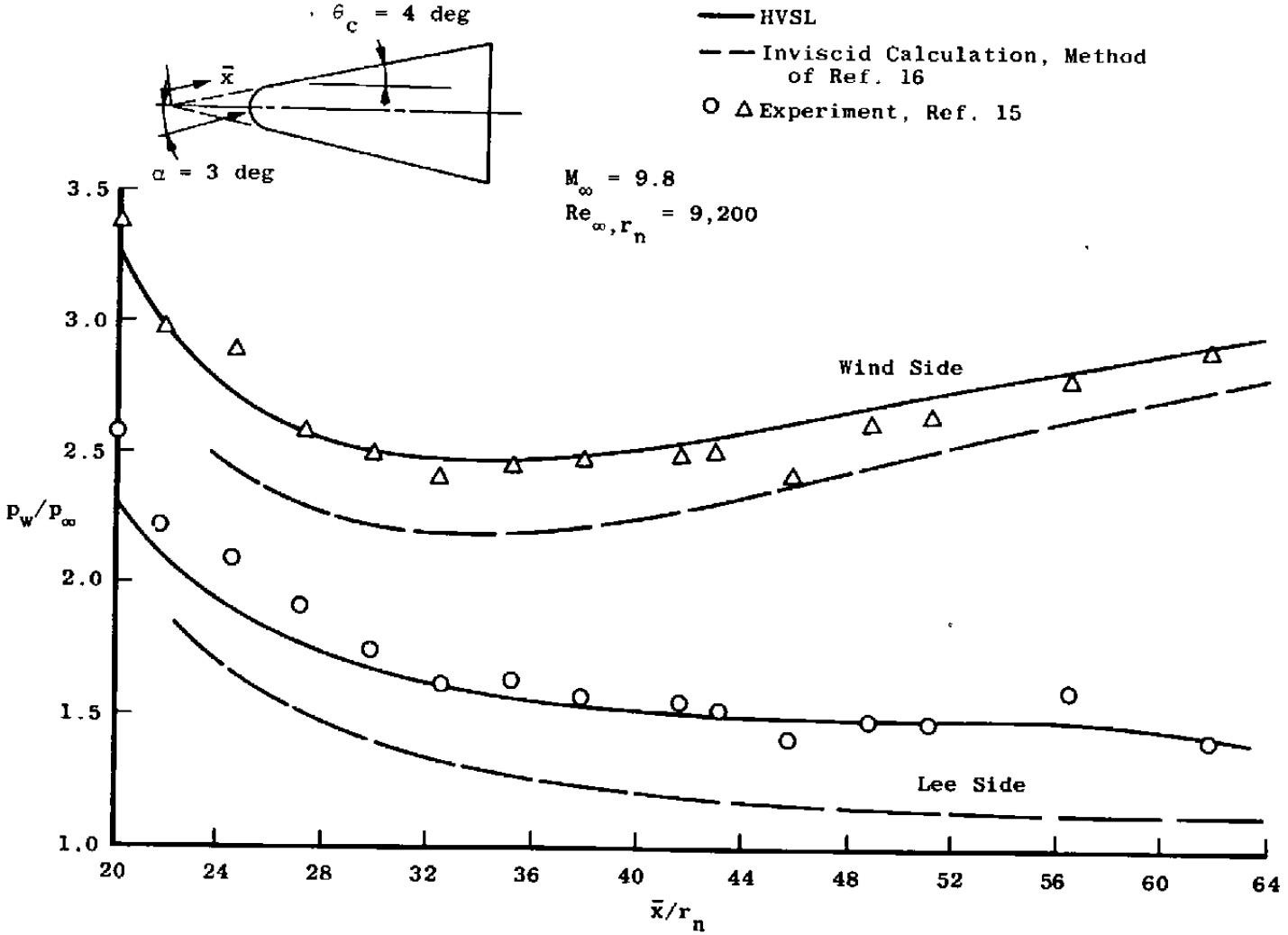

Figure 8. Surface pressure distribution along a 4-deg sphere cone at 3-deg angle of attack.

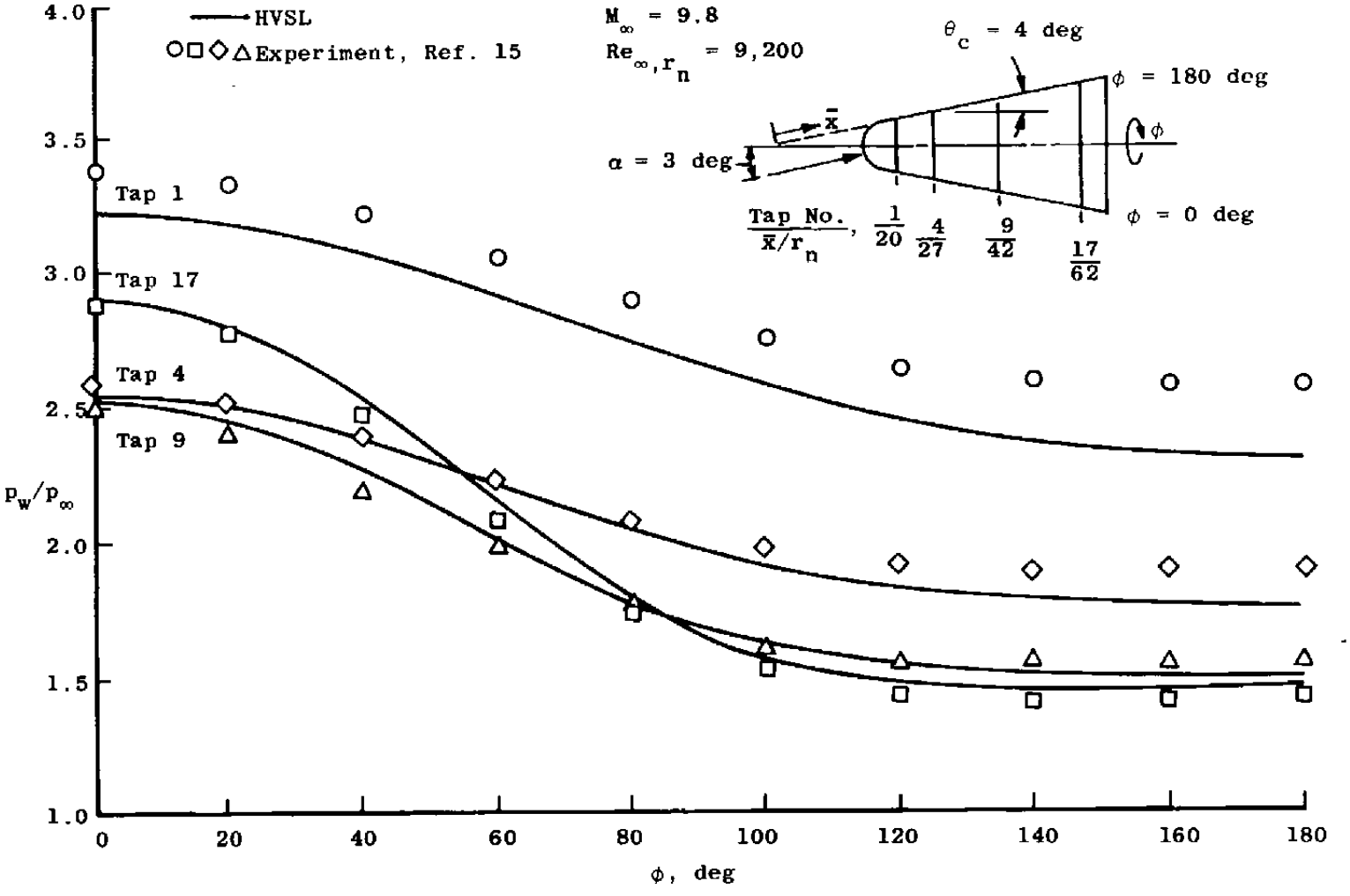

Figure 9. Surface pressure distribution around a 4-deg sphere cone at 3-deg angle of attack.

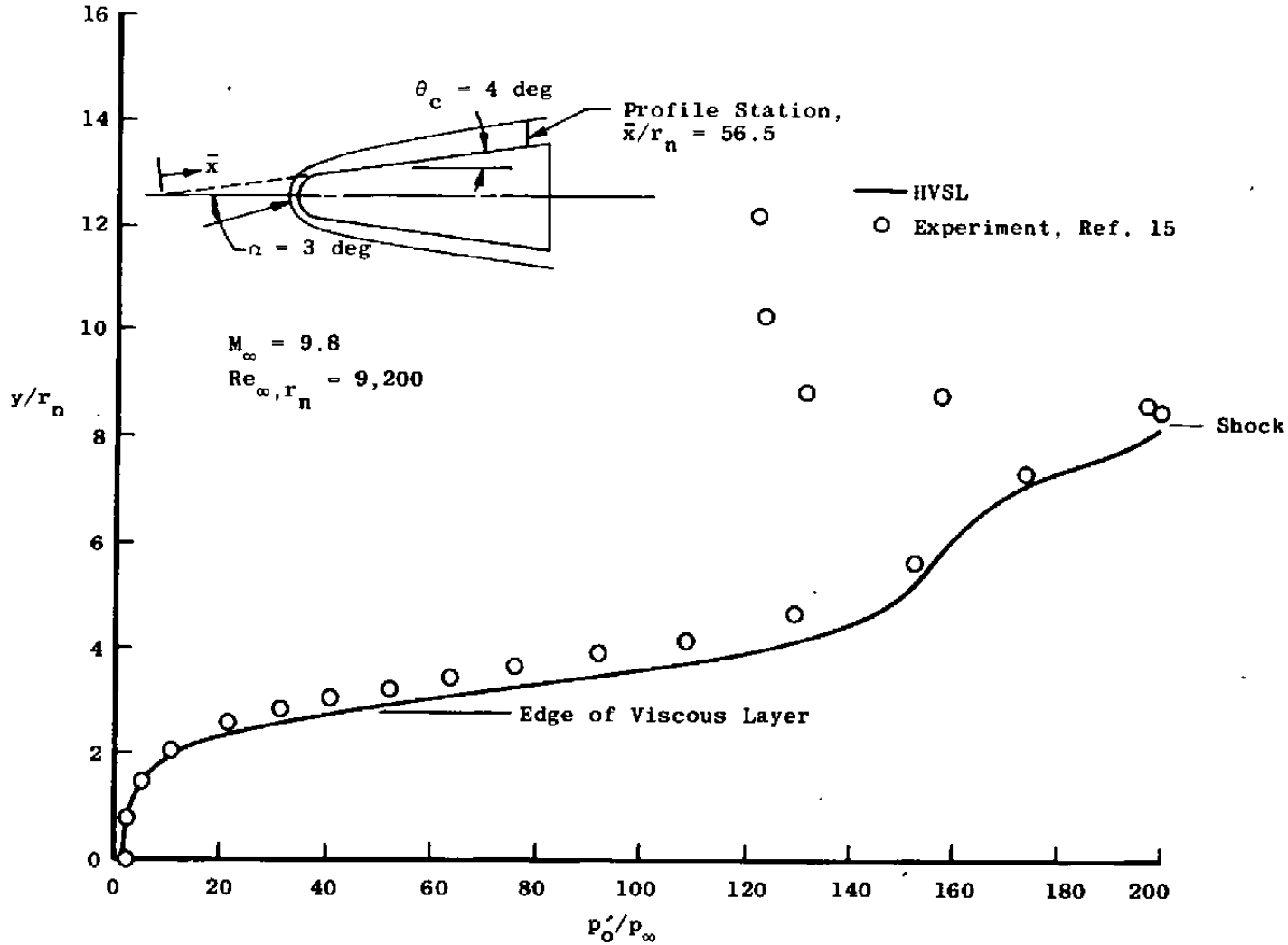

Figure 10. Lee-side pitot pressure profile on a 4-deg sphere cone at 3-deg angle of attack.

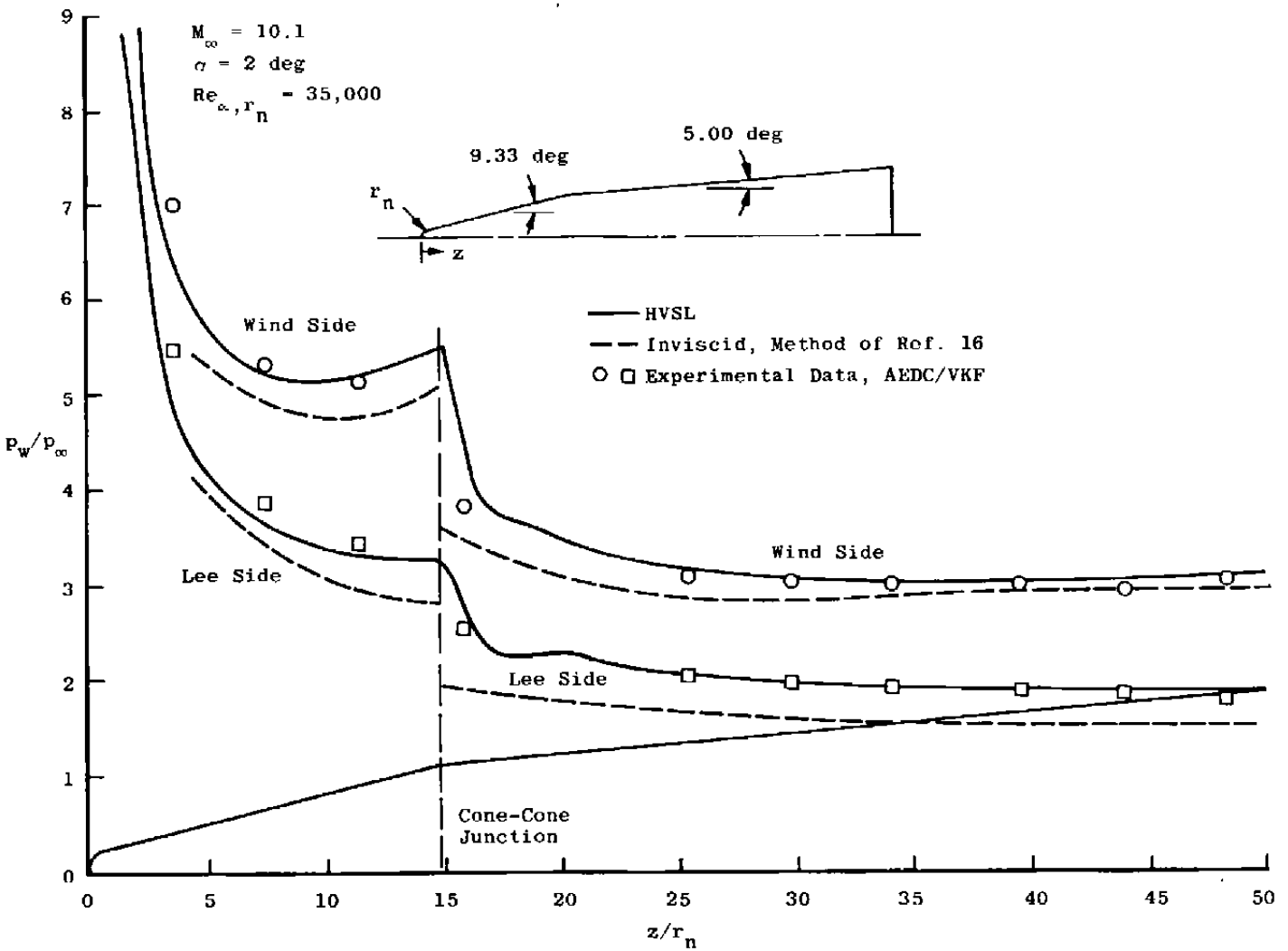

Figure 11. Blunt biconic longitudinal surface pressure distribution.

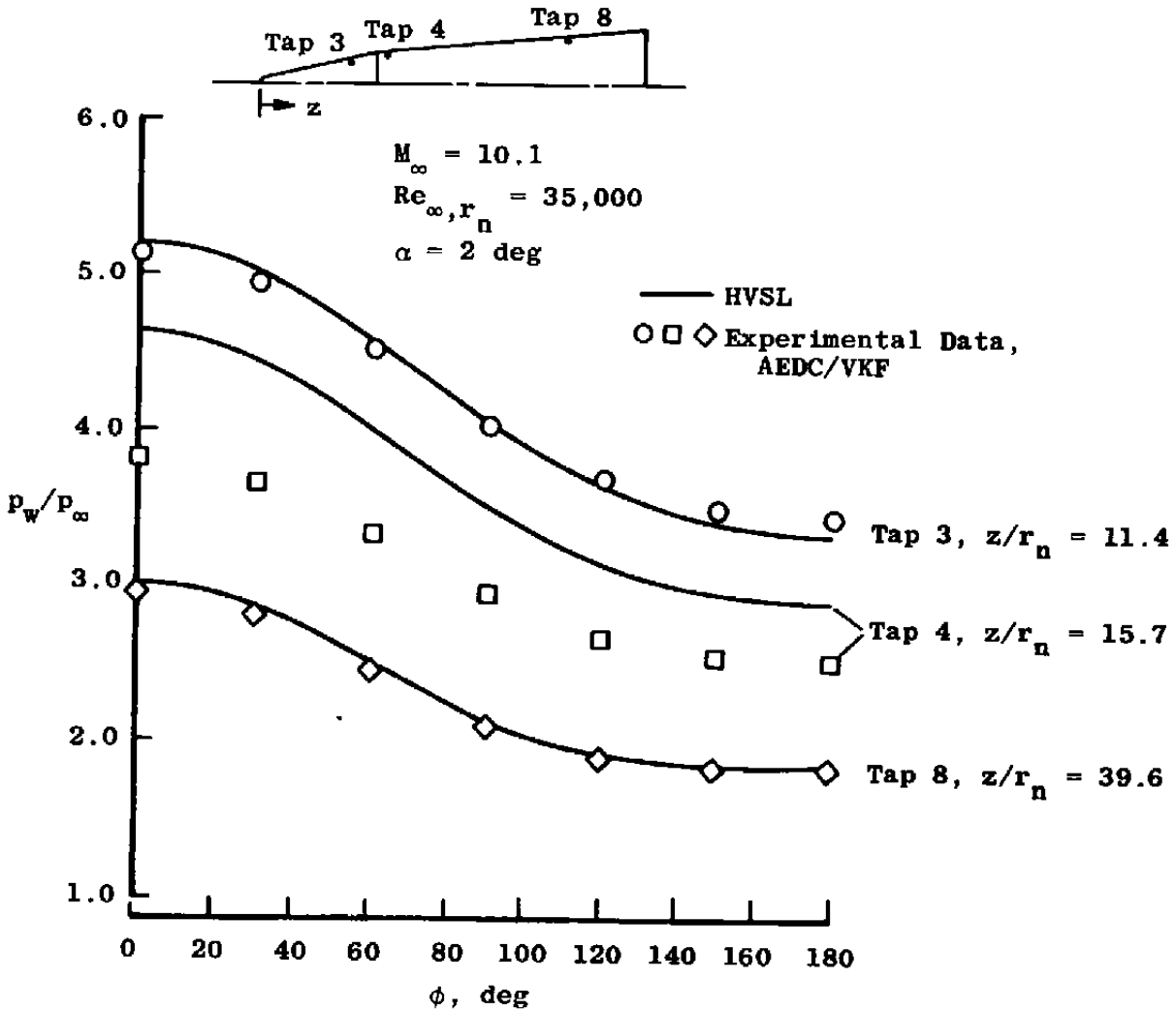

Figure 12. Blunt biconic circumferential surface pressure distribution.

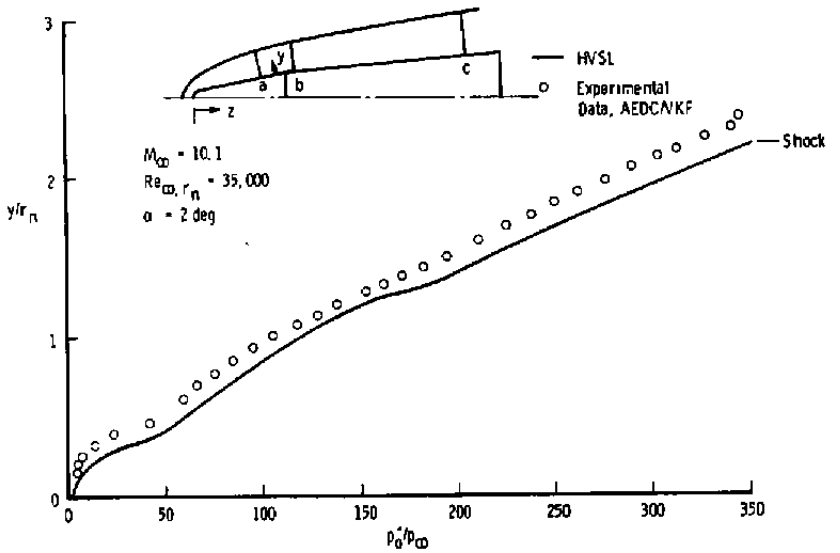

a. z/r_n = 11.4

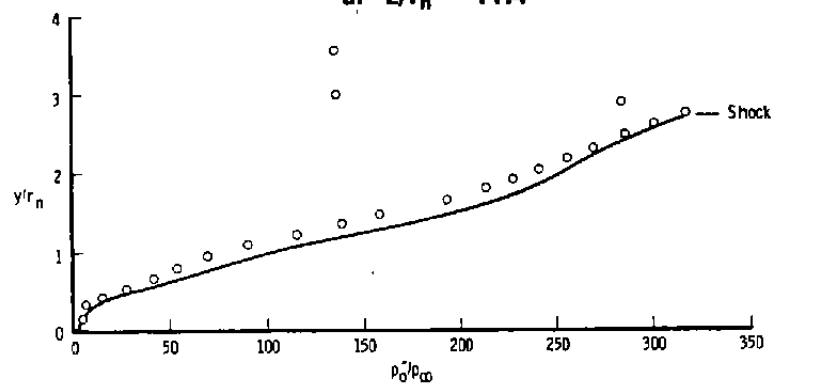

b. z/r_n = 15.7

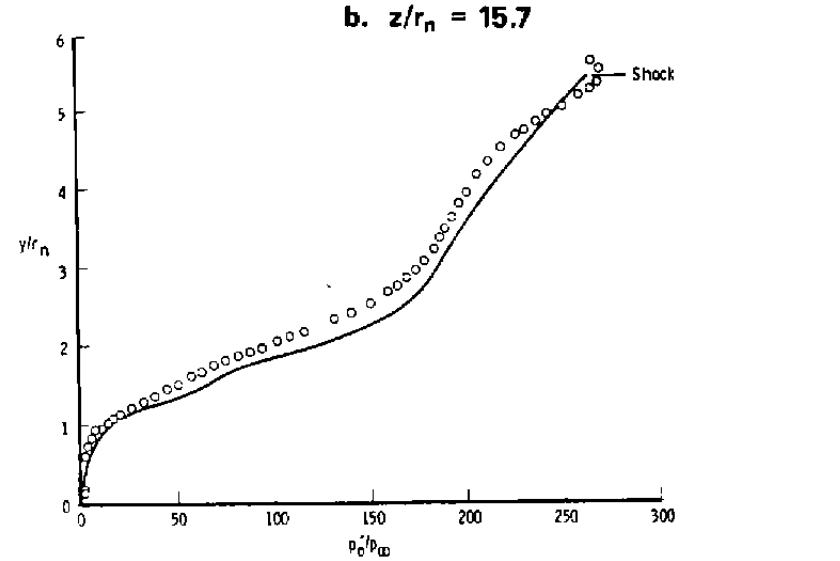

c. z/r_n = 39.6

Figure 13. Blunt biconic lee-side pitot pressure profiles.

NOMENCLATURE

h	Heat-transfer coefficient
h_o	Reference heat-transfer coefficient
h_w	Wall static enthalpy
H	Total enthalpy
H_∞	Free-stream total enthalpy
HVSL	Hypersonic Viscous Shock Layer code (Ref. 8)
L	Body axial length
M_∞	Free-stream Mach number
p	Static pressure
p_w	Wall static pressure
p_∞	Free-stream static pressure
p_o'	Pitot pressure
Pr	Prandtl number
$\dot{q}_w$	Wall heat-transfer rate
r	Radius about axis of symmetry
r_n	Spherical nose radius
Re_{∞, r_n}	Free-stream Reynolds number based on nose radius
s	Surface distance
St_∞	Stanton number based on free-stream conditions, $St_\infty = \dfrac{\dot{q}_w}{\rho_\infty U_\infty (H_\infty - h_w)}$

u	x component of velocity
U_∞	Free-stream velocity
v	y component of velocity
x	Coordinate along body surface
$\overline{x}$	Surface distance from virtual apex of sphere cone
y	Coordinate normal to body surface
y_{sh}	Value of y at shock wave
z	Axial distance from nose of body
α	Angle of attack
γ	Ratio of specific heats
θ_c	Cone frustum half-angle
θ_1	Fore-cone half-angle
θ_2	Aft-cone half-angle
κ	Longitudinal curvature
μ	Viscosity
ρ	Mass density
ρ_∞	Free-stream mass density
ϕ	Angular position around body from wind side